Journal of Infrastructure Planning and Engineering

Journal homepage: https://ejournal.warmadewa.ac.id/index.php/jipe

Validation control in finite element analysis of wide beam-column connections using concrete damage plasticity under cyclic loading

Putu Ayu Priska Dewi[1*], I Ketut Sudarsana[2], I Gede Adi Susila[2]

[1]*Magister of Civil Engineering Udayana University, Jl. PB Sudirman, Denpasar, 80113, Indonesia*
[2]*Department of Civil Engineering Udayana University, Bukit Jimbaran, Badung, 80361, Indonesia*
[*]dewipriska4@gmail.com

Received on 26 April 2025, accepted on 30 April 2025

ABSTRACT

This study investigates the validation of a finite element model for exterior wide beam–column connections using the Concrete Damage Plasticity (CDP) approach under reversed cyclic loading. The research focuses on identifying optimal CDP parameters—mesh size, dilation angle, and viscosity—through a structured trial-and-error process to enhance simulation accuracy. Using the SPWWS specimen as a benchmark, the final model configuration (40 mm mesh, 40° dilation angle, and 0.005 viscosity) produced peak load errors of 3.47% (positive) and 8.73% (negative) compared to experimental data. The simulation also replicated key damage mechanisms including diagonal, flexural, and torsional cracking observed in the laboratory test. These results validate the effectiveness of the calibrated CDP model in capturing both global and local nonlinear behaviors of RC joints under seismic loading. The validated model offers a reliable basis for future studies on reinforced concrete joints under modified loading conditions or strengthening interventions.

Keywords: concrete damage plasticity; validation control; finite element analysis; wide beam-column connection; cyclic loading

1 Introduction

Reinforced concrete (RC) wide beam–column connections have gained popularity in modern multistory buildings due to their architectural efficiency, economic formwork systems, and reduced overall building height [1], [2]. These connections are typically characterized by beam widths exceeding those of the supporting columns, creating geometric discontinuities that affect the joint's ability to transfer seismic forces effectively [3]. While codes such as SNI 2847:2019 [4], ACI 318-14 [5], and ACI 352R-02 [6] provide general guidelines for joint detailing, they are largely based on data from conventional narrow-beam configurations and do not fully account for the complex behavior of wide beam–column joints (WBCJs) under cyclic loading [7].

Numerous experimental studies have reported that even code-conforming WBCJs often experience premature failure due to torsional cracking of the spandrel beam, joint shear degradation, or poor anchorage of longitudinal reinforcement placed outside the column core [8], [9]. These damage mechanisms significantly reduce the energy dissipation capacity of the joint, compromising its seismic resilience [10]. The role of torsion in the spandrel beam has been recognized as a critical factor, influencing both strength and ductility of the connection [11].

Recent parametric investigations have highlighted that the detailing of spandrel beams, such as their depth, reinforcement ratio, and torsional stiffness, has a direct impact on the failure mode of WBCJs [12]. Deep or well-confined spandrels mitigate torsional failure and enable plastic hinging within the beam, consistent with strong-column–weak-beam behavior. Conversely, inadequate confinement or under-detailed spandrels tend to initiate brittle shear-torsion failures, especially under high drift levels [9], [11].

To better understand these failure mechanisms and evaluate code limitations, researchers have employed nonlinear finite element analysis (FEA) using the Concrete Damage Plasticity (CDP) model [13]. This model simulates cracking, stiffness

degradation, and energy dissipation behavior under cyclic loading, and has been calibrated to reproduce hysteretic curves, plastic hinge formation, and crack patterns observed in full-scale tests [14], [15]. In particular, studies have shown that model sensitivity to parameters such as dilation angle, viscosity coefficient, and tensile/compressive damage evolution requires careful validation to ensure convergence and accuracy [16].

However, one major challenge in numerical modeling lies in capturing the bond-slip behavior of reinforcement located outside the column face, a zone where experimental results have shown frequent early deterioration [8], [17]. Additionally, the definition of "effective beam width" contributing to flexural resistance remains ambiguous. Analytical studies suggest that current code limits may underestimate or overestimate this parameter, failing to reflect the torsional interactions that arise in wide spandrels [18].

In response to these issues, this study aims to establish a validated CDP-based FEA framework for simulating the seismic behavior of exterior WBCJs. The model will be benchmarked against published experimental data, with emphasis on force–deformation accuracy, failure mode replication, and validation of key response parameters. Furthermore, this study proposes practical recommendations for controlling validation quality in CDP-based modeling and identifying critical parameters that affect the joint performance, with the goal of improving the reliability of numerical simulation in seismic design of RC wide beam–column systems.

2 Data and Methods

2.1 Specimen Description

The specimen used for numerical validation in this study is the SPWWS exterior wide beam-column connection tested by Pakzad and Khanmohammadi [1]. The specimen was constructed at a 3:5 reduced scale and features a column cross-section of 250 mm × 250 mm and a wide beam section of 700 mm × 200 mm. In addition, spandrel beams with a cross-section of 650 mm × 200 mm were provided to extend 400 mm beyond the edge of the wide beam, ensuring proper anchorage for longitudinal reinforcement.

The clear span of the wide beam from face-to-face of columns was 1500 mm. The top and bottom reinforcement of the wide beam consisted of 11D10 and 8D10 bars, respectively, while the spandrel beams were reinforced with 9D12 bars at the top and 6D12 bars at the bottom. The column was reinforced with 12D12 longitudinal bars, and closed ties were provided using D10 stirrups. The specimen layout, reinforcement details, and section cuts are illustrated in Figure 1, adapted from the original experimental study [1].

The concrete had a compressive strength $(f'c)$ of 29.3 MPa, while the reinforcement had yield strengths ranging from 462 MPa to 568 MPa. The material properties are summarized in Table 1.

2.2 Finite Element Modeling

The numerical model was developed using ABAQUS/Standard. The concrete elements were modeled with 8-node linear brick elements (C3D8R) using reduced integration, while the reinforcing bars were represented by 2-node linear truss elements (T3D2), embedded within the concrete matrix using the embedded region constraint technique. In this study assumes a perfect bond between the reinforcement and concrete. Figure 2 and Figure 3 presents the associated mesh configuration and reinforcement details.

To replicate the boundary conditions used in the experimental testing, a coupling constraint was applied at the ends of the column and beam elements, connecting their end surfaces to corresponding reference points. The boundary conditions were then enforced at these reference points.

The lower end of the column was modeled as a pinned support, allowing rotational movement but restricting translational displacements.

The upper end of the column was kept free, enabling both vertical displacement (to simulate axial load application) and lateral displacement under cyclic loading.

At the end of the spandrel beams, the displacement was constrained to allow movement only in the horizontal direction, while vertical movement was restricted to mimic the support conditions in the experimental setup. The overall boundary condition configuration used in this study is illustrated in Figure 4.

A constant axial load equivalent to 15% of the gross column axial capacity $(0.15A_g f'c)$ was applied throughout the cyclic loading test. The axial load was introduced through a reference point coupled to the top surface of the column and maintained constant during the entire analysis under force-controlled conditions.

Following the application of axial load, lateral cyclic displacements were imposed at the top reference point of the column. The lateral loading protocol consisted of two cycles per drift level up to 1% drift and three cycles beyond 1%, in accordance with quasi-static testing standards. Each drift level was subjected to multiple repeated cycles to assess strength degradation and stiffness deterioration under cyclic loading. The lateral displacements increased incrementally in successive drift levels. The complete drift loading sequence applied in the simulation is outlined in Figure 5.

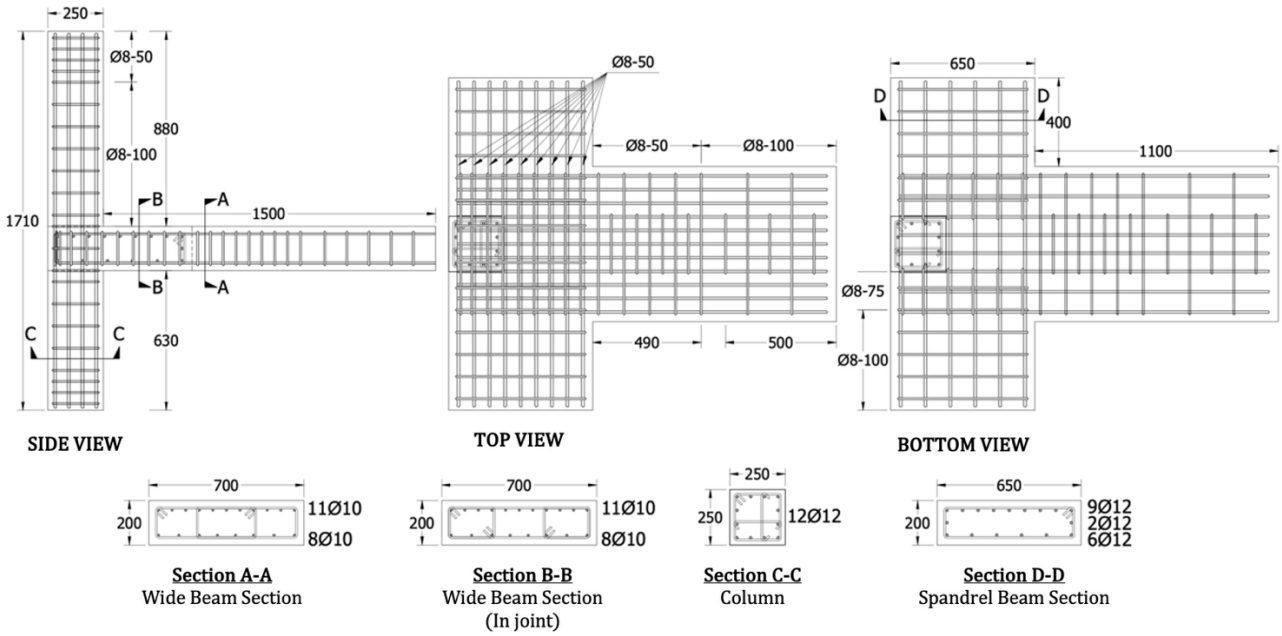

Figure 1. Dimensions and reinforcement model (in mm)

Table 1. Material properties

Concrete	Reinforcement					
f'_c (MPa)	Diameter (mm)	Use Reinforcement	f_y (MPa)	f_u (MPa)	ε_y (%)	ε_u (%)
29,3	8	Transversal	530	749	0,255	13,8
	10	Longitudinal	462	575	0,221	11,6
	12	Longitudinal	568	761	0,275	11,1

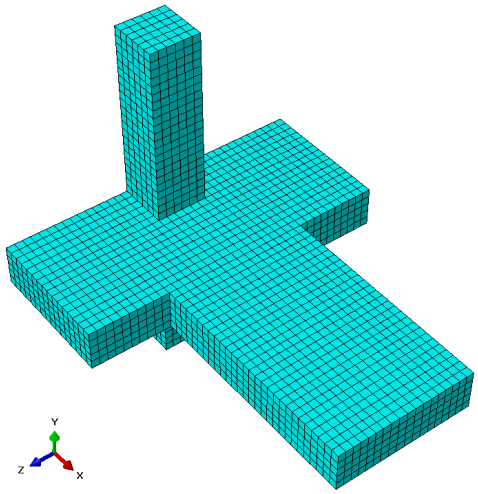

Figure 2. Geometric model in FEM

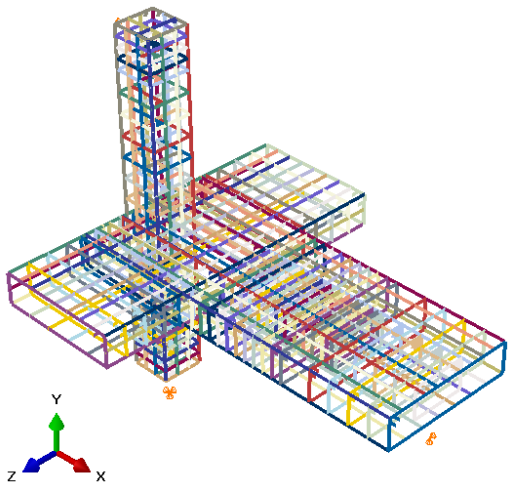

Figure 3. Reinforcement model in FEM

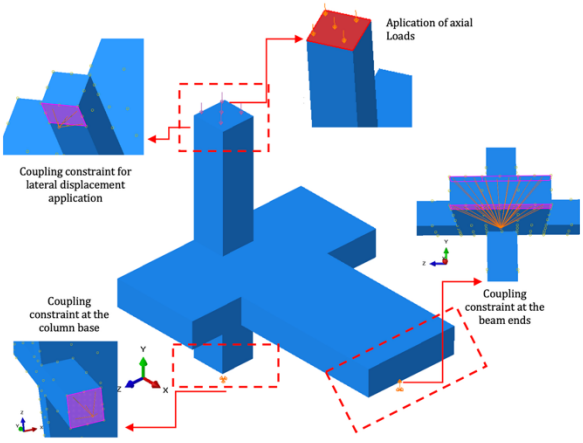

Figure 4. Boundary condition and loading setup

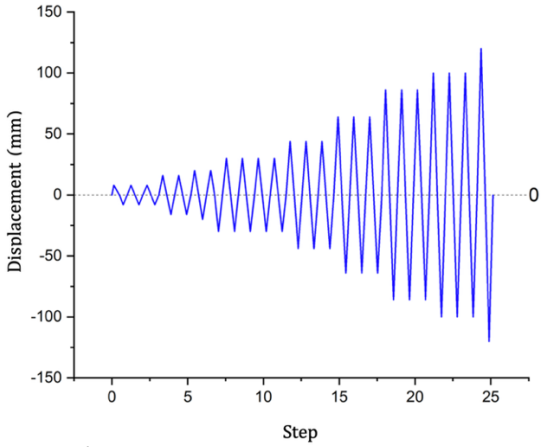

Figure 5. Cyclic loading protocol

2.3 Concrete Damage Plasticity Model

Concrete nonlinear behavior was simulated using the Concrete Damage Plasticity (CDP) model. The initial selection of CDP parameters was based on recommendations from previous studies that highlighted their significant impact on the accuracy of numerical models.

The control parameters investigated in this study included the dilation angle, viscosity parameter, and mesh size. A systematic investigation was conducted by varying the mesh size from 30 mm to 50 mm, the dilation angle from 25° to 40°, and the viscosity parameter from 0 to 0.0009, while maintaining constant values for eccentricity (0.1), the stress ratio of biaxial to uniaxial compressive strength (1.16), and the shape factor Kc (0.67).

Calibration was performed through a manual trial-and-error procedure by observing the effects of each parameter adjustment on critical response indicators, such as the lateral load-displacement relationship, crack pattern development, ultimate load capacity, and failure mode characteristics.

Iterative adjustments continued until the numerical simulation adequately replicated the experimental backbone curve shape and failure mechanism observed in the SPWWS specimen test [1].

2.4 Validation Process

The validation process utilizes ABAQUS finite element software with an automated control approach. As shown in Figure 6, the process begins with preprocessing in ABAQUS/CAE, where the model geometry, material properties, CDP parameters, boundary conditions, and loading protocol are defined through input control. During the simulation phase in ABAQUS/Standard, the control system monitors parameter sensitivity, convergence criteria, and solution stability. This phase generates output files including job.odb, job.dat, job.res, and job.fil. The final stage involves postprocessing in ABAQUS/CAE, where automated result extraction, data comparison, and error analysis are performed to validate the numerical model against experimental data. This systematic control approach ensures consistent validation procedures and efficient parameter optimization.

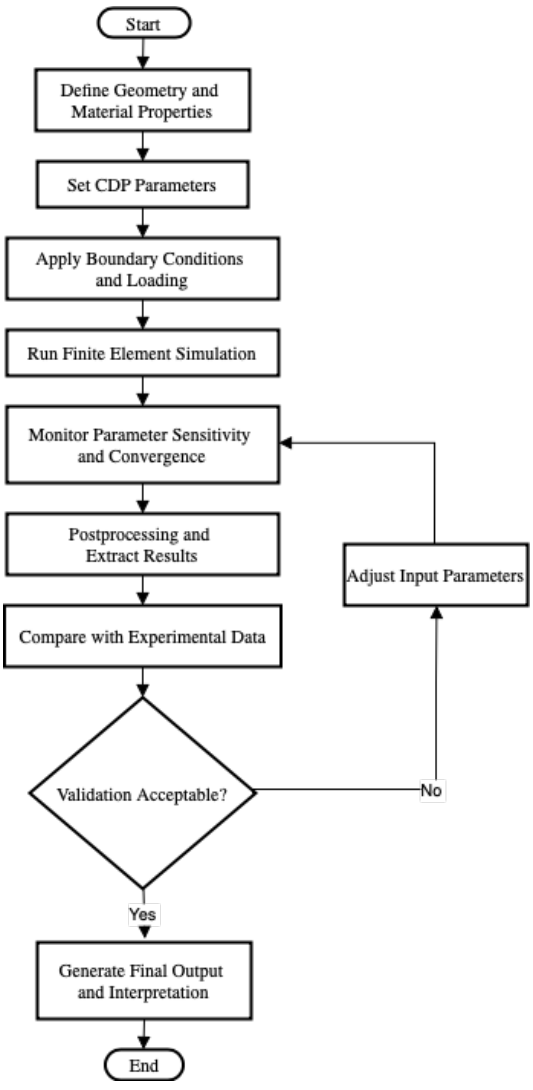

Figure 6. Validation process flow diagram

3 Results and Discussion

3.1 Concrete Damage Plasticity (CDP) Parameter Control

In order to achieve a reliable finite element model, three critical parameters influencing the Concrete Damage Plasticity (CDP) behavior were systematically investigated: mesh size, dilation angle, and viscosity parameter.
Each parameter was varied individually while keeping the other parameters constant to isolate its effect on the lateral load-deformation response of the wide beam-column connection.

Mesh Size Control

Figure 7 illustrates the backbone curves generated using five different mesh sizes ranging from 30 mm to 70 mm and Table 2 summarizes the validation results comparing the finite element predictions and experimental ultimate lateral strengths for different mesh sizes.

Among all the models, the simulation using a 40 mm mesh size demonstrated the best agreement with experimental results, achieving an error of 7.8% for positive loading and 0.21% for negative loading. Models with finer meshes (30 mm) exhibited slightly larger errors, particularly in the positive direction (8.8%), while coarser meshes (50–70 mm) led to significantly higher deviations, reaching up to 14.8% for positive and 12.9% for negative loading.

These results confirm that a 40 mm mesh size provides an optimal balance between numerical accuracy and computational efficiency. Furthermore, finer meshes did not significantly improve the predictive accuracy, while coarser meshes tended to overestimate structural stiffness and underestimate crack propagation, leading to lower accuracy in replicating experimental behavior.

Table 2. Comparison mesh size variation

Mesh Size (mm)	FEM Result		Eror
	Force (kN)	Drift (%)	(%)
30	31.103	6.691	8.80
	-54.527	-8.036	2.60
40	31.429	7.975	7.80
	-56.115	-8.003	0.21
50	30.350	8.008	11.00
	-5.,713	-8.001	5.87
60	29.051	7.999	14.80
	-49.404	-7.967	11.78
70	29.752	7.990	12.74
	-48.816	-7.895	12.86

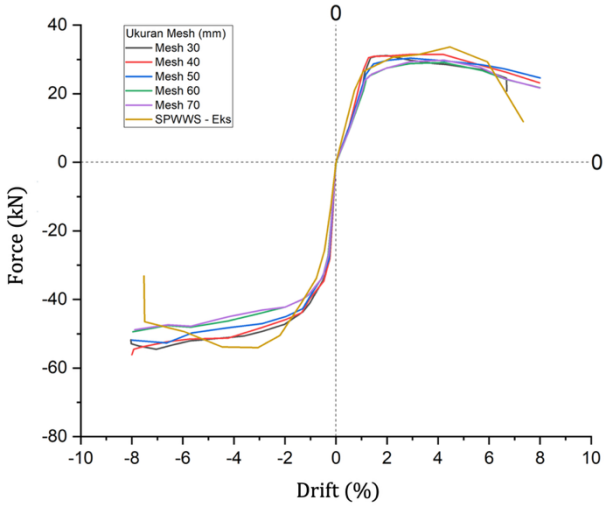

Figure 7. Backbone curve of mesh size variation effect

Dilation Angle Control

The variation of dilation angle was found to significantly affect the lateral load response of the reinforced concrete connection model.

As illustrated in Figure 8, increasing the dilation angle resulted in a noticeable enhancement in the simulated backbone curve, with better alignment to the experimental response. A dilation angle of 40° produced the most optimal prediction, with a peak lateral load of 34.34 kN in the positive direction and −50.34 kN in the negative direction.

This corresponds to the smallest prediction error, as summarized in Table 3, with only 0.15% deviation in the positive direction compared to the experimental maximum load of 34.1 kN. Although the error in the negative direction reached 10.1%, it remains acceptable for nonlinear modeling of RC joints.

Table 3. Comparison dilation angle variation

Dilation Angel (ψ)	FEM Result		Eror (%)
	Force (kN)	Drift (%)	
25°	30.582	6.663	10.30
	-50.014	-4.259	10.7
30°	31.259	5.694	8.33
	-50.590	-5.709	9.66
35°	32.575	6.518	4.48
	-50.288	-4.214	10.2
40°	34.342	5.702	0.15
	-50.340	-4.209	10.1

In contrast, lower dilation angles such as 25° and 30° led to reduced lateral strength and stiffer responses, diverging further from the experimental trend. This behavior reflects a more brittle response

under cyclic loading, which may underestimate damage evolution and energy dissipation capacity. These results confirm that higher dilation angles enhance ductility and better simulate the inelastic behavior of concrete under cyclic loading.

Overall, the analysis validates that a 40° dilation angle provides the best balance between numerical performance and physical accuracy for the CDP model used in this study.

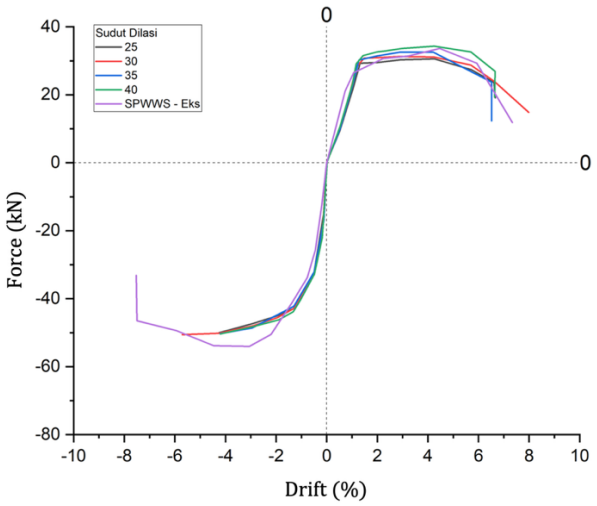

Figure 8. Backbone curve of dilation angle variation effect

Viscosity Parameter Control

The effect of the viscosity parameter (μ) on the simulated behavior of the reinforced concrete connection was investigated to improve numerical stability and match the cyclic response more accurately. As shown in Figure 9, varying the viscosity parameter significantly influenced the smoothness and convergence of the backbone curves, though with marginal effects on the overall strength values.

According to Table 4, the model with (μ) = 0.005 exhibited a well-balanced performance, yielding peak lateral loads of 32.92 kN (positive) and −51.11 kN (negative). This configuration provided acceptable accuracy while maintaining computational stability, with predicted strengths relatively close to the experimental values of 34.1 kN and −56.0 kN, respectively.

In contrast, the model without viscosity (μ = 0) resulted in abrupt strength fluctuations and a stiffer response in the positive direction (35.56 kN), leading to an underestimation of nonlinear deformation characteristics.

Similarly, values of (μ) = 0.0009 and (μ) = 0.001 slightly overestimated the stiffness and strength, especially in the negative direction. These results demonstrate that introducing a moderate viscosity parameter (μ = 0.005) enhances the convergence behavior of the CDP model under cyclic loading without excessively damping the mechanical response. Therefore, (μ = 0.005) was adopted in the final model as the most suitable value for capturing the inelastic behavior realistically while ensuring numerical efficiency.

Table 4. Comparison viscosity parameter variation

Viskositas (μ)	FEM Result		Eror (%)
	Force (kN)	Drift (%)	
0	35.559	4.306	4.27
	-51.155	-4.292	8.66
0,001	30.156	4.310	11.54
	-49.293	-4.293	12.01
0,005	32.917	4.303	3.46
	-51.110	-4.299	8.73
0,0009	35.580	4.303	4.35
	-52.950	-4.300	5.45

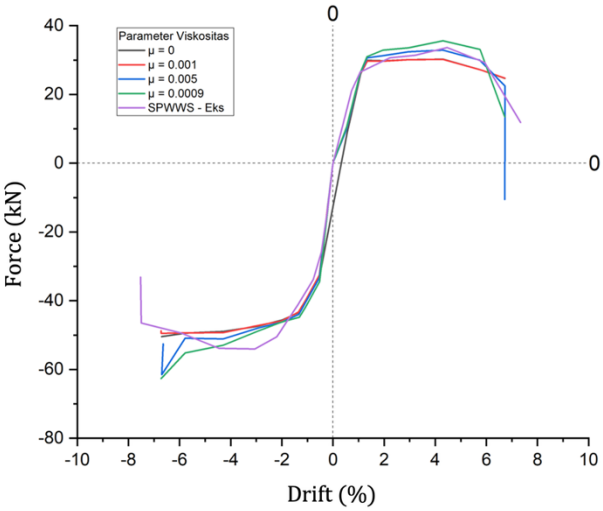

Figure 9. Backbone curve of viscosity parameter variation effect

3.2 Validation Results

Load-Deformation Comparison

Following the calibration of CDP parameters through mesh size, dilation angle, and viscosity sensitivity analysis, the final finite element model was validated using the integrated parameter set, as shown in Table 5. The comparison between experimental and numerical load–deformation responses is presented in Figure 10, and the corresponding quantitative results are summarized in Table 6.

The numerical simulation yielded peak lateral loads of 32.92 kN (positive) and −51.11 kN (negative), compared to the experimental values of 34.1 kN and −56.0 kN. This resulted in error values of 3.47% and 8.73%, respectively, indicating strong correlation between the numerical and experimental data. Drift

values were also closely matched, with the FEM model producing maximum displacements of 4.303% and −4.299%, compared to 4.5% and −4.5% from the experimental test.

The shape of the backbone curve in Figure 11 confirms that the model accurately captured both the strength and stiffness degradation observed under cyclic loading. These findings validate that the selected parameter combination in the CDP model successfully simulates the behavior of exterior wide beam–column connections, particularly in reproducing peak strength, drift demand, and nonlinear post-peak behavior.

Table 5. Validated CDP and Structural Sensitivity Parameters Used in the Final Numerical Model

Failure Parameter	Value
Dilation Angle (ψ)	40°
Eccentricity (ϵ)	0.1
Stress Ratio $(\sigma_{b0}/\sigma_{c0})$	1.16
Shape Factor (K_c)	0.667
Viscosity Parameter (μ)	0.005
Mesh Size (mm)	40

Table 6. Numerical-experimental comparison and validation error

Exp. Result		FEM Result		Eror
Force (kN)	Drift (%)	Force (kN)	Drift (%)	(%)
34.1	4.5	32.917	4.303	3.47
-56.0	-4.5	-51.110	-4.299	8.73

Damage Pattern Validation Confirms

The validation of the damage pattern was carried out by comparing the numerical simulation results with the experimental observations, as shown in Figure 12. The damage contours were extracted based on the tensile damage variable in the CDP model, which effectively visualizes crack initiation, propagation, and failure distribution throughout the joint region.

In the initial phase, diagonal cracks appeared on the wide beam edge and extended toward the column face at deformation levels below 1%, accurately representing the first cracking observed experimentally. As deformation increased to around 1.5%, cross-cracks developed on the lateral face of the spandrel beam adjacent to the column, with crack widths intensifying at higher drift levels. Flexural cracks were observed at both the top and bottom edges of the wide beam, while the column exhibited minimal flexural damage, indicating that it remained within the elastic range during the analysis. In terms of torsional response, torsional cracking occurred on the spandrel beam within a region approximately equal to the column depth, suggesting the occurrence of pure torsion along a length matching the height of the column. By the end of the analysis, cracks had spread across the entire connection region, indicating a global distribution of damage.

The overall failure mode and cracking pattern from the numerical model closely resembled the experimental specimen, reinforcing the validity of the CDP-based simulation in replicating realistic structural behavior under cyclic loads.

This strong correlation between damage visualization and physical crack development confirms the ability of the CDP model to accurately simulate both strength and failure mechanisms in exterior wide beam–column connections.

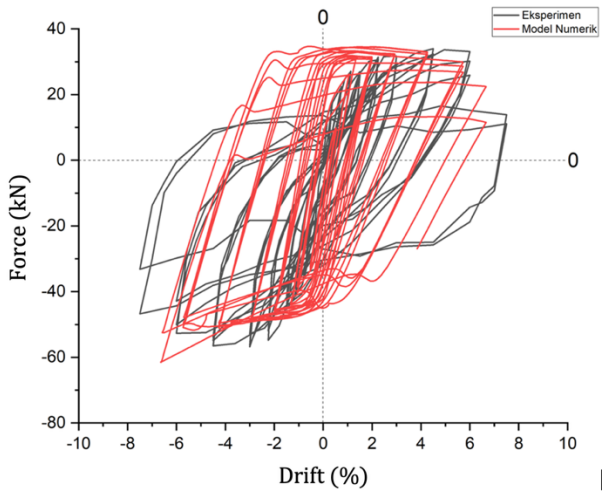

Figure 10. Hysteretic response under cyclic loading: experimental vs FEM

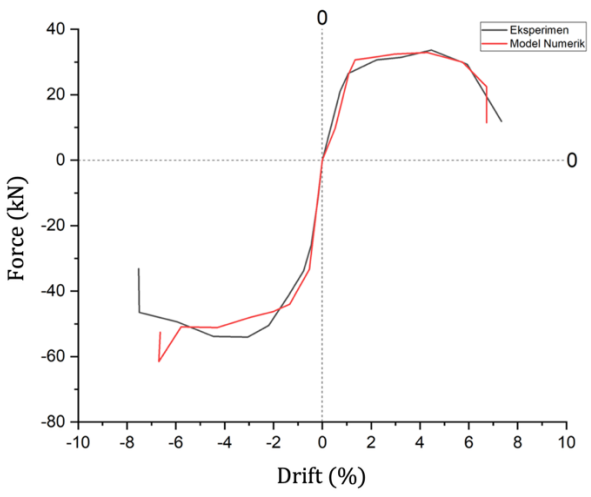

Figure 11. Backbone curve: experimental vs FEM

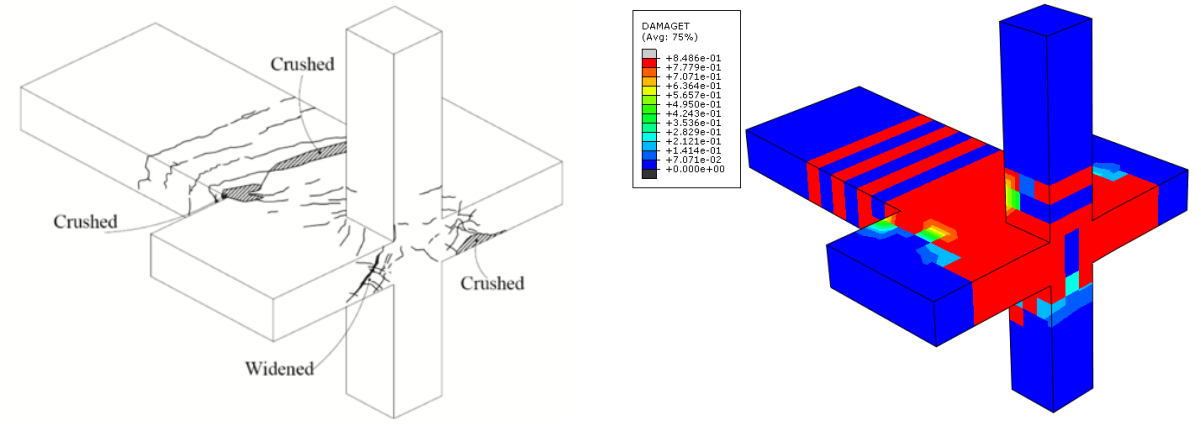

a. Experimental crack overview (sketch)

b. Numerical tensile damage contour – global view

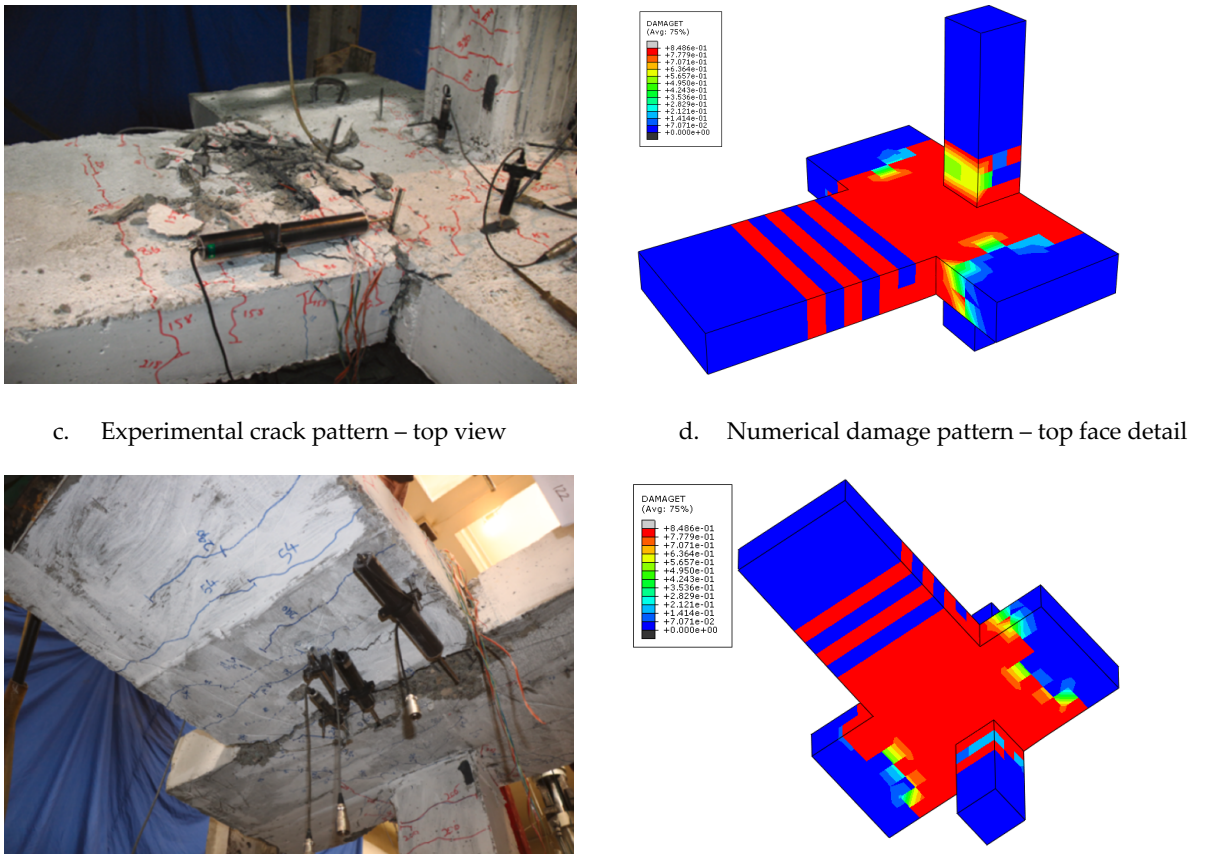

c. Experimental crack pattern – top view

d. Numerical damage pattern – top face detail

e. Experimental crack pattern – bottom view

f. Numerical damage pattern – bottom face detail

Figure 12. Comparison between experimental and numerical crack patterns at final loading cycle

4 Conclusion

This study has successfully validated a finite element model of exterior wide beam–column connections using the Concrete Damage Plasticity (CDP) approach under cyclic loading. Through sensitivity analyses of three critical parameters—mesh size, dilation angle, and viscosity coefficient—the most effective configuration was identified. The selected parameters, namely a 40 mm mesh size, 40° dilation angle, and 0.005 viscosity, produced simulation results with excellent agreement to experimental data, showing load prediction errors of 3.47% in the positive direction and 8.73% in the negative direction.

The model was able to replicate the full load–deformation response of the tested specimen, including peak strength, stiffness degradation, and post-peak behavior. Moreover, the CDP-based simulation successfully captured key damage

mechanisms, such as diagonal cracking in early stages, flexural cracking at beam ends, and torsional damage at the spandrel beam near the column face. These findings affirm the effectiveness of the selected CDP parameters in reproducing both global and local structural behavior.

Looking forward, future studies may consider extending the validated CDP model to simulate reinforced concrete joints under varying axial load ratios, confinement levels, or retrofitted conditions. This includes evaluating the effect of strengthening strategies, geometric modifications, or multi-hazard scenarios. As highlighted in the work of [19], changes in structural demands—such as those caused by vertical expansions—require capacity reassessment and may benefit from numerical modeling of strengthening techniques like FRP applications. These directions will broaden the applicability of validated CDP-based finite element models in modern structural design and retrofit analysis.

References

[1] A. Pakzad and M. Khanmohammadi, "Experimental cyclic behavior of code-conforming exterior wide beam-column connections," Engineering Structures, vol. 214, 2020, doi: 10.1016/j.engstruct.2020.110613.

[2] H. Behnam, J. S. Kuang, and B. Samali, "Parametric finite element analysis of RC wide beam-column connections," Computers and Structures, vol. 205, pp. 28–44, 2018, doi: 10.1016/j.compstruc.2018.04.004.

[3] V. V. S. and N. Mohan, "Exterior Type-2 Wide Beam-Column Connection: An Overview," International Journal of Scientific & Engineering Research, vol. 11, no. 10, pp. 200–206, 2020.

[4] Badan Standardisasi Nasional, SNI 2847:2019 – Persyaratan Beton Struktural untuk Bangunan Gedung, Jakarta, Indonesia, 2019.

[5] ACI Committee 318, Building Code Requirements for Structural Concrete (ACI 318-19) and Commentary, American Concrete Institute, 2019.

[6] ACI Committee 352, Recommendations for Design of Beam-Column Connections in Monolithic Reinforced Concrete Structures (ACI 352R-02), American Concrete Institute, Farmington Hills, MI, USA, 2002.

[7] R. Y. C. Huang and J. S. Kuang, "Predicting strength of exterior wide beam–column joints for seismic resistance," Journal of Structural Engineering, ASCE, vol. 146, no. 2, 2020, doi: 10.1061/(ASCE)ST.1943-541X.0002488.

[8] G. Santarsiero and A. Masi, "Key mechanisms of the seismic behaviour of external RC wide beam–column joints," The Open Construction and Building Technology Journal, vol. 13, pp. 36–51, 2019, doi: 10.2174/1874836801913010036.

[9] R. Y. C. Huang, J. S. Kuang, and H. Behnam, "Shear strength of exterior wide beam-column joints with different beam reinforcement ratios," Journal of Earthquake Engineering, 2018, doi: 10.1080/13632469.2018.1545711.

[10] H. Behnam and J. S. Kuang, "Exterior RC wide beam–column connections: Effect of spandrel beam on seismic behavior," Journal of Structural Engineering, ASCE, vol. 144, no. 4, 2018, doi: 10.1061/(ASCE)ST.1943-541X.0001995.

[11] S. H. Luk and J. S. Kuang, "Seismic performance and force transfer of wide beam–column joints in concrete buildings," Proceedings of the Institution of Civil Engineers – Engineering and Computational Mechanics, vol. 170, no. EM2, pp. 71–88, 2017, doi: 10.1680/jencm.15.00024.

[12] E. Etemadi and T. Vincent, "Mechanical behavior of RC exterior wide beam–column joints under lateral loading: A parametric computational study," International Journal of Engineering and Technology, vol. 9, no. 3, pp. 2003–2012, 2018, doi: 10.21817/ijet/2017/v9i3/1709030153.

[13] H. Behnam, J. S. Kuang, and Q. Huang, "Reinforced concrete exterior wide and conventional beam-column joints under earthquake-type loading," 16th World Conference on Earthquake Engineering (16WCEE), Santiago, Chile, 2017.

[14] G. Santarsiero and A. Masi, "Finite element analysis of external RC wide beam–column joints provided with different detailing solutions," in COMPDYN 2017 – 6th ECCOMAS Thematic Conference on Computational Methods in Structural Dynamics and Earthquake Engineering, Rhodes Island, Greece, 2017, doi: 10.7712/120117.5699.17312.

[15] E. Etemadi and K. Fallahnezhad, "Behavior of reinforced concrete interior wide beam–column connections under lateral loading: A finite element study," International Journal of Engineering and Technology, vol. 9, no. 3, pp. 2559–2570, 2017, doi: 10.21817/ijet/2017/v9i3/1709030061.

[16] E. Etemadi and T. Vincent, "Mechanical behavior of RC exterior wide beam–column joints under lateral loading: A parametric computational study," International Journal of Engineering and Technology, vol. 9, no. 3, pp. 2003–2012, 2017, doi: 10.21817/ijet/2017/v9i3/1709030153.

[17] M. Hafezolghorani, F. Hejazi, R. Vaghei, M. S. Jaafar, and K. Karimzade, "Simplified damage plasticity model for concrete," Structural Engineering International, vol. 27, no. 1, pp. 68–78, 2017, doi: 10.2749/101686616X1081.

[18] J. S. Kuang, H. Behnam, and Q. Huang, "Effective beam width of reinforced-concrete wide beam–column connections," Proceedings of the Institution of Civil Engineers – Structures and Buildings, 2017, doi: 10.1680/jstbu.15.00124.

[19] I. W. M. Andreasnata, I. N. Sinarta, N. K. Armaeni, I. P. E. Sarassantika, D. T. Trung, C. B. Casita, R. Sulaksitaningrum, and S. P. Tampubolon, "Column structure strengthening with FRP due to story addition," Journal of Infrastructure Planning and Engineering (JIPE), vol. 1, no. 1, pp. 38–45, Apr. 2022, doi: 10.22225/jipe.1.1.2022.38-45.